Steps towards de-novo life

Monreal Santiago, Guillermo

DOI:
10.33612/diss.121581426

Chapter 5

Towards an autonomous chemical oscillator

In this chapter, we use the photosensitizer Rose Bengal, introduced in Chapter 4, to engineer a negative feedback loop in our system of peptide-based self-replicators. As expected from the quantum yields of singlet oxygen formation described in the previous chapter, photocatalytic oxidation can be inhibited by the formation of the replicator. This process, which slows down replication, is the core of the design of a novel potential chemical oscillator. We describe a series of steps that have been taken towards the experimental realization of this oscillator. First, we have used a model compound to prove that out-of-equilibrium formation of disulfides is possible in a photooxidation-reduction regime. Secondly, we have studied individual reactions that, combined, provide all the required ingredients for an oscillator: a positive feedback loop, a negative one, and a delay between them due to different reactivities with a reducing agent. Lastly, we have used a kinetic model to show that damped oscillations are possible in this system within experimentally reasonable parameters.

5.1 Introduction

The objective of the previous chapters was to recreate some of the properties of life in synthetic systems. In doing so, we developed a chemical reaction network (CRN) that combines different feedback loops, based on a peptide-based replicator ($\mathbf{1}_6$) and a photocatalyst (**2**). Chemical reaction networks are known to exhibit emergent properties [1] such as bistability [2–6], pattern formation [7, 8], and oscillations [9–12]. Extensive theoretical work has been done to predict how the topologies of such CRNs relate to the emergent properties that arise from them, with an emphasis on the design of oscillators [10, 11, 13–17].

The first requirement for CRNs to show sustained oscillations is to be in out-of-equilibrium conditions [10]. Closed systems tend towards an energy minimum, so a constant influx of energy and/or matter is necessary to keep the system in a state of constant change. The way this has been approached experimentally for most reported oscillators [2, 6, 15, 18, 19] is the use of a continuous stirred-tank reactor (CSTR), where the products are constantly removed from the solution and new material (normally, in the form of precursors) is added at the same rate to keep the total concentration constant. When an autocatalytic reaction is ran in a CSTR, it can lead to bistability: the existence of two different steady states in exactly the same experimental conditions, where the system selects one or the other depending on the initial concentration of the autocatalytic species. Bistability is not intrinsically necessary for oscillations, however it is closely related to them: oscillators can be constructed starting from a bistable system and introducing an element that perturbs the system differently in each of the states [2, 10]. Another approach for reaching the required out-of-equilibrium conditions is the constant inflow of a reagent that destroys the oscillating species and transforms it back into its precursors. Oscillations have been achieved in these semi-batch conditions, although they were damped over time [20].

Once that autocatalysis is kept out of equilibrium in an open system, a number of network topologies can give rise to sustained oscillations. One of those topologies, supported by both theoretical [11, 17] and experimental [19] studies, combines a positive and a negative feedback loop, the second one being delayed in time.

A close examination of the network introduced in Chapter 4 shows two positive feedback loops: the autocatalytic effect of $\mathbf{1}_6$ in its own formation from $\mathbf{1}_3/\mathbf{1}_4$, and its activation of **2**, which catalyses the photooxidation of **1** to $\mathbf{1}_3/\mathbf{1}_4$. However, as explained in that chapter, the activation of **2** by $\mathbf{1}_6$ is the net result of two effects: a large increase in its absorbance, which enhances its photocatalytic activity, and a smaller reduction of its $^1O_2$ formation quantum yield (Φ_Δ), which reduces it. If the increase in absorbance was cancelled, we could transform the second positive feedback loop in a negative one - potentially leading to the emergence of oscillatory behaviour in the $\mathbf{1}_6$ system.

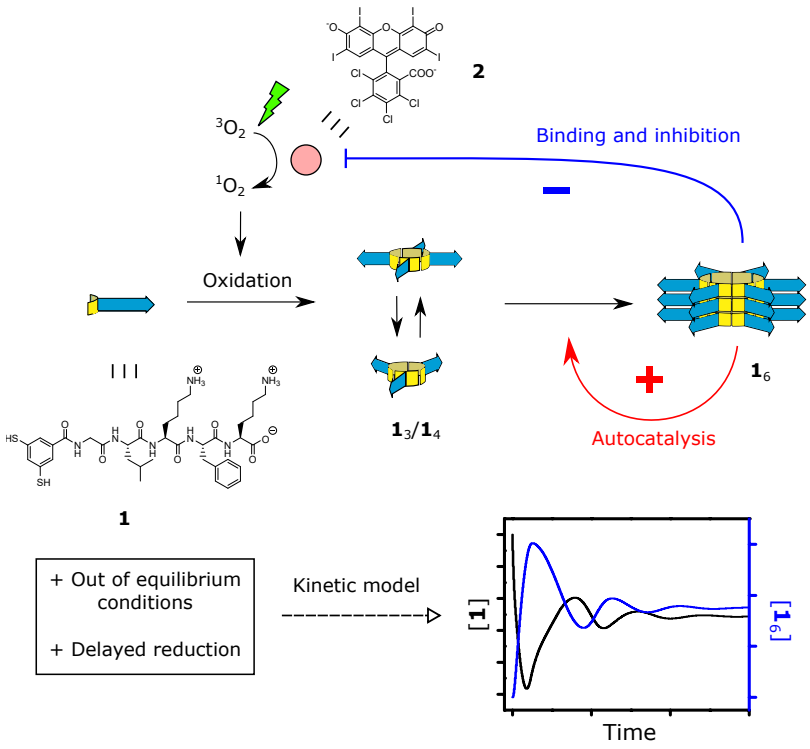
2
$^3O_2$
$^1O_2$
Binding and inhibition
Oxidation
$\mathbf{1}_3/\mathbf{1}_4$
$\mathbf{1}_6$
Autocatalysis
1
+ Out of equilibrium conditions
+ Delayed reduction
Kinetic model
[1]
[$\mathbf{1}_6$]
Time

5.2 Preliminary results

As mentioned in the introduction, in order to design an oscillator based on the self-replicator $\mathbf{1}_6$ we need to keep the system out of equilibrium. Since $\mathbf{1}_6$ is based on disulfide bonds, we decided to achieve this by using photooxidation and a constant inflow of a reducing agent. To the best of our knowledge, there is no precedent in the literature of disulfides being formed in out-of-equilibrium conditions in this way, so our first step was to establish this methodology. The system based on **1** is inherently complicated, consisting of a number of macrocycles that exchange and interact with one another, changing the rates of the photooxidation and reduction reactions with their relative concentrations. This complexity is necessarily for the oscillator, as explained below, but it complicates the study of its individual reactions. For that reason, we decided to use a model compound to study the basic features of the out-of-equilibrium mechanism: the kinetics of both photooxidation and reduction, and whether it is possible to reach a steady state of disulfides in this formation-destruction regime.

We chose the thiol **5** (2-nitro-5-thiobenzoate, which dimer is commonly known as Ellmann's reagent [21]) as a model compound (Figure 5.1). Its structure is relatively similar to **1**, but it only has one thiol and therefore it cannot form species larger than a dimer. This made it a good candidate for our preliminary experiments, together with its easy analysis due to a large difference in the UV spectra of its monomeric and dimeric forms (Figure S5.1).

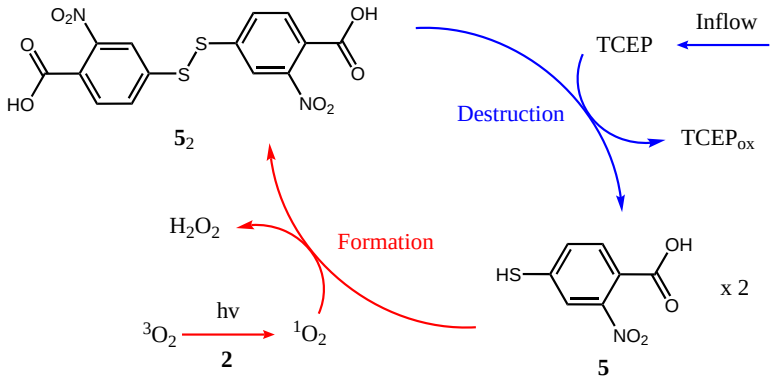

Figure 5.1: Scheme of the reactions leading to the out-of-equilibrium formation of $\mathbf{5}_2$.

First, we studied the formation and destruction pathways separately. Destruction proceeded through reduction with TCEP as described previously [22]: following the second order kinetics that can be expected from an S_N2 reaction (Figures 5.2a and S5.3) The photooxidation of **5**, using **2** as a photocatalyst and a 525 nm LED as an irradiation source, proceeded without a significant amount

of side-products (Figure S5.2), and had a first order dependence on the concentration of **5** (Figures 5.2b and S5.3). Its reaction order in **2** was not constant for the range of concentrations studied, indicating different rate determining steps at different concentrations.

Next, we combined both reactions by setting an experiment with both photooxidation and TCEP inflow. In these conditions, we observed a steady state in the concentration of **5** (Figure 5.2c). Interestingly, when both reduction and oxidation were switched off at the same time, the system kept being reduced, indicating the presence of unreacted TCEP in the solution. This indicates that, in this regime, $^1O_2$ and TCEP are primarily reacting with **5** and $\mathbf{5}_2$ and not directly with each other.

Reduction	
Reagent	Reaction order
$\mathbf{5}_2$	1.02±0.02
TCEP	0.9±0.1

(a) Experimentally determined reaction orders in the reduction of $\mathbf{5}_2$

Oxidation	
Reagent	Reaction order
5	1.04±0.07
2	*

(b) Experimentally determined reaction orders in the photooxidation of **5**

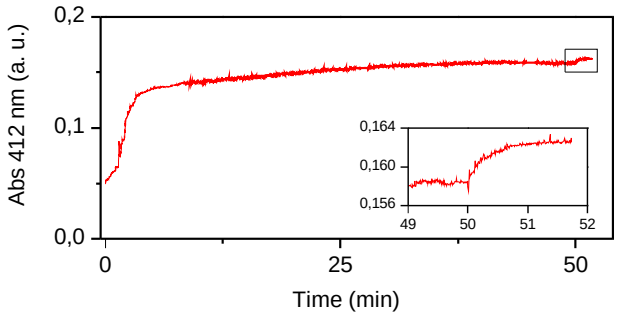

(c) Out-of-equilibrium formation of $\mathbf{5}_2$ in a photooxidation-reduction regime

Figure 5.2: Kinetic studies on the dissipative formation of $\mathbf{5}_2$ disulfides by photooxidation and reduction. (a) and (b): Reaction orders of the individual reagents in each of the reactions. The reaction order of **2** was not constant for the range of concentrations studied (See *Methods* and Figure S5.3 for the calculations). (c): Steady state in the formation of $\mathbf{5}_2$ disulfides. The initial concentrations were 100 µM of $\mathbf{5}_2$ and 10 µM of **2**, and borate buffer was used as a solvent (pH = 8.2, 50 mM). The irradiation source was a 525 nm LED, and TCEP was flown in at an initial rate of 24 µM/min. After 2 minutes, the inflow rate was reduced to 1.2 µM/min. Finally, both irradiation and inflow of reducing agent were completely stopped after 50 minutes.

5.3 Results and discussion

Negative feedback loop and delay: The effect of $\mathbf{1}_6$ in photooxidation and reduction

As discussed in Chapter 4, the quantum yield of the formation of singlet oxygen (Φ_Δ) by **2** is reduced in presence of $\mathbf{1}_6$ fibres. For the wavelength used in that chapter (590 nm), the increase in absorbance of **2** in presence of $\mathbf{1}_6$ fibres is so large that the overall effect is still an increase in oxidation rate, which leads to $\mathbf{1}_6$ formally catalysing the formation of $\mathbf{1}_3/\mathbf{1}_4$. However, for wavelengths where the absorbance of **2** does not change upon the addition of $\mathbf{1}_6$, it can be expected that the change in Φ_Δ will be the dominating effect - so $\mathbf{1}_6$ will instead inhibit oxidation (Figure 5.3a and Figure 5.3b).

This was indeed the case when irradiating **1** + **2** samples using a LED with an emission wavelength of 525 nm. In these conditions, our experiments showed a ~2x fold (2.1 ± 0.5) decrease in the oxidation rate of **1** when $\mathbf{1}_6$ was present (Figures 5.3c and 5.3d).[1] This effect should lead to a negative feedback loop - as $\mathbf{1}_6$ inhibits the oxidation of **1** to $\mathbf{1}_3/\mathbf{1}_4$, which in turn slows down the formation of $\mathbf{1}_6$ itself. As it was shown in Chapter 1, the formation of $\mathbf{1}_6$ is autocatalytic, so in this case a positive and a negative feedback loop would be combined: $\mathbf{1}_6$ would both catalyse and inhibit its own formation.

As discussed in the introduction, the combination of a positive and a negative feedback loop is necessary to have sustained oscillations, in this case of the concentration of $\mathbf{1}_6$. However, it is not sufficient: in order to achieve oscillations, there should be a delay between the two cycles and the system should be operated in out-of-equilibrium conditions. A constant influx of reducing agent should accomplish these two purposes. On one hand, it will constantly drive the system towards the formation of **1**, allowing for the formation of disulfides only when there is a high enough photooxidation rate. On the other, the reduction of small macrocycles such as $\mathbf{1}_3$ and $\mathbf{1}_4$ should be significantly faster than the reduction of $\mathbf{1}_6$, as most of the disulfide groups in the latter are shielded by the self-assembled structure. In this way, $\mathbf{1}_3/\mathbf{1}_4$ can act as a buffer between the emergence of $\mathbf{1}_6$ and its reduction.

We tested this experimentally with two different reducing agents: TCEP and DTT. Our results show that the reduction rate of $\mathbf{1}_6$ is indeed slower than the reduction rate of $\mathbf{1}_3/\mathbf{1}_4$ with both of them, although the difference is much more

[1] Surprisingly, when no preoxidized $\mathbf{1}_n$ macrocycles were added to the sample, we observed an initial increase in the absorbance at 350 nm (the wavelength used to monitor the concentration of **1**, see Figure S5.4) before it started decreasing. It is impossible that **1** is being formed in these conditions, therefore this probably indicates the formation of an intermediate that either has a different absorbance, or changes the absorbance of **2**. In any case, since samples containing only **1** were not very relevant for this work (as $\mathbf{1}_3/\mathbf{1}_4$ will always be present as soon as the oxidation starts), we did not investigate this phenomenon any further

pronounced in the case of DTT (Figure S5.5). A possible explanation for this difference in behaviour is the electrostatic binding between the negatively-charged TCEP and $\mathbf{1}_6$ fibres, which would increase its local concentration and compensate for the decrease in rate due to protection within the self-assembled structure. The reduction rate of $\mathbf{1}_6$ fibres increased when the fibres had been mechanically shortened (Figure S5.6), indicating that their reduction rate can also be controlled through the amount of mechanical stress applied to the sample.

Conditions	Φ_Δ
2	0.76
2 + $\mathbf{1}_3/\mathbf{1}_4$	0.37
2 + $\mathbf{1}_6$	0.12

(a) Quantum yields of singlet oxygen formation of **2** in presence of different $\mathbf{1}_n$ macrocycles

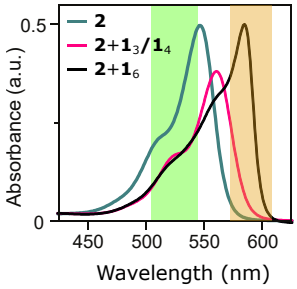

(b) Spectra of **2** + $\mathbf{1}_n$ macrocycles and emission of the LEDs used here and in Chapter 4.

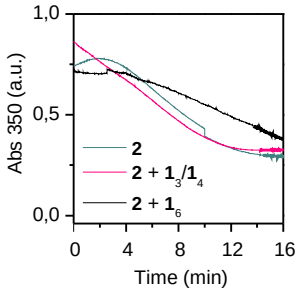

(c) Photooxidation of **1** in presence of different $\mathbf{1}_n$ macrocycles under irradiation with 525 nm light.

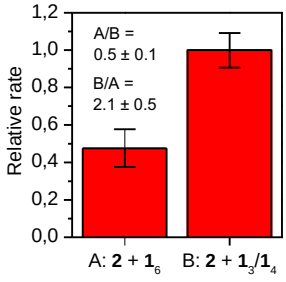

(d) Relative photooxidation rates in presence of different $\mathbf{1}_n$ macrocycles under 525 nm irradiation.

Figure 5.3: Inhibition of the photocatalytic activity of **2** by the addition of $\mathbf{1}_n$ macrocycles. (a) Φ_Δ of **2** in presence of $\mathbf{1}_3/\mathbf{1}_4$ and $\mathbf{1}_6$. (b) UV-Vis absorption spectra of **2** (4.0 µM) in presence of different $\mathbf{1}_n$ macrocycles (80 µM). (c) Absorbance at 350 nm over time of **1** (200 µM) samples irradiated with 525 nm LEDs, at 25 °C in presence of **2** (4.0 µM) and either $\mathbf{1}_3/\mathbf{1}_4$ or $\mathbf{1}_6$ (200 µM). The absorbance at this wavelength is mainly due to **1** (Figure S5.4). (d) Relative initial photooxidation rates of **1** samples prepared in the conditions of (c). The error bars represent the standard deviation of three samples. The data in (a) and (b) was taken from Chapter 4. All the samples were prepared in borate buffer (pH = 8.2, 50 mM).

Oscillator design

The combination of the results shown above led us to believe that the system of **1** and **2** can lead to oscillations when set up under irradiation with 525 nm light and with continuous inflow of a reducing agent:

1. If the irradiation and the inflow are set in such a way that the rate of oxidation (r_{ox}) is similar to, but slightly higher than the rate of reduction (r_{red}), $\mathbf{1}_3/\mathbf{1}_4$ will initially accumulate.

2. Once that they have reached a certain concentration, $\mathbf{1}_6$ will emerge and start self-replicating.

3. Upon the emergence of $\mathbf{1}_6$, **2** will bind to it, decreasing its Φ_Δ and therefore r_{ox}.

4. If the initial r_{ox} was close enough to r_{red}, this might cause a change in the conditions of the system, going from a net oxidation to a net reduction.

5. First, mainly $\mathbf{1}_3/\mathbf{1}_4$ will be reduced, giving $\mathbf{1}_6$ some extra time to keep growing. However, eventually the $\mathbf{1}_3/\mathbf{1}_4$ concentration will be low enough for $\mathbf{1}_6$ to start being reduced to **1** as well.

6. Upon reduction of $\mathbf{1}_6$, the Φ_Δ of **2** will increase again, restoring the oxidative conditions and returning the system to its initial state.

Let us add one last remark about this design. As indicated in the introduction, out-of-equilibrium conditions are critical for oscillations to emerge. The *Preliminary results* of this chapter (Section 5.2) shows that achieving an out-of-equilibrium regime is indeed possible for disulfides subjected to photooxidation and reduction. As shown in Figure 5.2c, disulfides can reach an actual steady state in these conditions, and not just an equilibrium where both TCEP and $^1O_2$ react completely as soon as they are added/generated: there is enough reducing agent present in the steady state to continue the reaction as soon as the external energy and material inputs are discontinued. We expect that the reactions with $\mathbf{1}_n$ macrocycles will show a similar behaviour and a steady state will be reached in this system as well.

Kinetic model

One of the main bottlenecks in the design of oscillators is the large parameter space that needs to be explored in order to locate the often small subset of conditions that harbours the oscillatory behaviour. The system described above involves a large number of variables, and even in the most optimistic scenario only a small number of combinations of those variables will lead to oscillations. In

order to determine if oscillations are possible at all, and to narrow the range of parameters to explore, we decided to simulate the system it using a kinetic model before developing it experimentally (Figure 5.4a, Table S5.1).

The first reaction of this model is the oxidation of **1** to small macrocycles (represented as only $\mathbf{1}_3$ for simplicity). The rate of this oxidation has a first order dependence on the concentration of **1** (as previous experiments indicate), and it depends on k_1, a value that starts as a constant but decreases as the concentration of $\mathbf{1}_6$ fibres grows (see below). To simplify the model, the concentration of $^1O_2$ (implicitly included in k_1) is assumed to be constant.

The next reactions are the reduction of $\mathbf{1}_3$ (modelled as a bimolecular second order reaction with DTT, since it is a thiol-disulfide exchange [23]), and a fast exchange between $\mathbf{1}_3$ and $\mathbf{1}_6$, modelled as second order reactions in both directions (based on previous theoretical knowledge of the system). The autocatalytic behaviour of $\mathbf{1}_6$ is modelled using two reactions that convert $\mathbf{1}_6$ into a second species, $\mathbf{1}_6^{fib}$. The first reaction is uncatalysed, and depends only on the concentration of $\mathbf{1}_6$, while the second one is catalysed by $\mathbf{1}_6^{fib}$. These two reactions represent two phenomena that we understand to be fundamental to the replication of $\mathbf{1}_6$: the nucleation of short fibres from unassembled $\mathbf{1}_6$ macrocycles, and the catalysed elongation of those fibres.

We added reactions representing the inflow of DTT from a stock solution, and the reduction of $\mathbf{1}_6$ and $\mathbf{1}_6^{fib}$. These reduction constants had the same value for $\mathbf{1}_3$ and $\mathbf{1}_6$, but the one corresponding to $\mathbf{1}_6^{fib}$ was 40 times lower. This represents how the fibre structure protects the disulfides of $\mathbf{1}_6$ (see above).

The inhibitory effect of $\mathbf{1}_6^{fib}$ in the photooxidation reaction (represented by k_8, a factor that multiplies the initial value in the formula of k_1) is critical for oscillations, but at the moment we lacked direct evidence on how to model it. Chemical intuition tells us that it depends on the number of **2** molecules bound to $\mathbf{1}_6$ fibres at each concentration, going from a maximum value at $[\mathbf{1}_6^{fib}] = 0$ to a minimum once that $[\mathbf{1}_6^{fib}]$ is enough to bind all of them. We decided to represent this as a linear decrease of k_8 with $\mathbf{1}_6^{fib}$ until k_8 had reached a certain value, and then as a constant.[2] We defined the slope of the initial decrease as k_9. At a constant concentration of **2**, this value represents the strength of its binding to $\mathbf{1}_6$: The higher k_9 is, the less $\mathbf{1}_6$ that is necessary to bind all **2** molecules.

Once that the model was completed, we needed to assign values to each rate constant. We decided to set their units so all concentrations would be relative to the total concentration of **1** building blocks. In that way, the concentrations in the model would range from 0 to 1 and the results could be extrapolated to different initial concentrations.

[2] In a future iteration of the model, the shape of this function could be determined more accurately by measuring the photooxidation rate of **1** at different **2** and $\mathbf{1}_6$ concentrations.

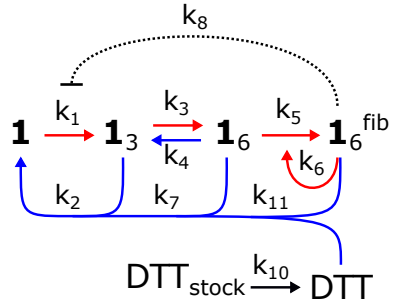

(a) Scheme of the model, including rate constants and other parameters.

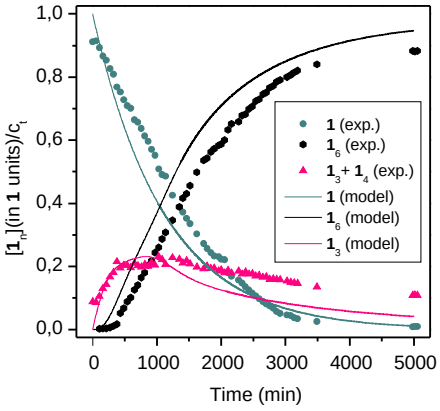

(b) Experimental values (symbols) and simulation (lines) of an experiment without photooxidation or reduction.

Formula or initial value	Units
$k_0 = 6 \times 10^{-4}$	min^{-1}
$k_1 = k_0 \times k_8$	min^{-1}
$k_2 = 6 \times 10^{-2}$	$c_t^{-1} min^{-1}$
$k_3 = 2 \times 10^{-2}$	$c_t^{-1} min^{-1}$
$k_4 = 2 \times 10^{-2}$	$c_t^{-1} min^{-1}$
$k_5 = 1 \times 10^{-2}$	$c_t^{-1} min^{-1}$
$k_6 = 1 \times 10^{-1}$	$c_t^{-1} min^{-1}$
$k_7 = k_2$	$c_t^{-1} min^{-1}$
$k_8 = 1 - k_9 \times [\mathbf{1}_6{}^{fib}]$ (min. 0.3)	Unitless
$k_9 = 20$	c_t^{-1}
$k_{10} = 6 \times 10^{-4}$	$c_t\ min^{-1}$
$k_{11} = k_2/40$	$c_t^{-1} min^{-1}$

(c) Definition of the constants and parameters used in the model

Figure 5.4: Description of the kinetic model used in this chapter and comparison with experimental values. (a): Scheme showing the reactions described in the model. (b): Dynamics of a **1** library (200 mM, pH = 8.2, 40 °C, stirred) compared to the simulated values ($k_0 = 3 \times 10^{-4}$, $k_9 = k_{10} = 0$, other constants as in (c)). (c): Values or equations defining all the parameters of the model. These values were kept through all simulations unless otherwise specified.

First, we set the values of constants related to "intrinsic" reactions of the system (k_3, k_4, k_5, k_6, and a "*sans*-photooxidation" k_0). For this, we took as a reference an experiment at 40 °C without any photooxidation or reduction, and assigned values to the constants to get a similar behaviour in the model (Figure 5.4b). These values were not thoroughly fitted, just estimated to get a model reasonably close to the experiment.[3] Once that these constants were determined, k_0 (the constant for initial oxidation) was doubled, to account for the effect of photocatalysis. Of course, this value is completely arbitrary, as the rate of photooxidation can be modified experimentally (by increasing the concentration of **2** and/or the intensity of the irradiation source), but we have observed in Chapter 4 that a photooxidation rate of twice the uncatalyzed value can be easily achieved and does not cause any side reactions, so we decided to use it as a starting point.

The value of k_2, which determines the rates of reduction (all other reduction constants are defined as fractions of k_2) was set to be slightly higher than the exchange constants, as DTT-based reduction is a disulfide exchange reaction itself. The minimum value of k_8 (representing a completely inhibited oxidation) was set to 0.3, roughly its theoretical minimum as Φ_Δ is three times lower in presence of $\mathbf{1}_6$ than in presence of $\mathbf{1}_3/\mathbf{1}_4$[4]. Most simulations in this chapter were done using this value instead of the experimentally determined 0.5 ± 0.1 (Figure 5.3d). As it will be shown later, the exact value of this parameter is critical in determining the behaviour of the system.

In order to estimate the value of k_9 - the decrease in Φ_Δ of **2** as $\mathbf{1}_6^{\text{fib}}$ increases, we used as a reference a UV titration of **2** with $\mathbf{1}_6$. As shown in Chapter 4, as the concentration of $\mathbf{1}_6$ increases the intensity of the band at 589 nm first increases and then decreases. If we assume that all **2** is bound at the point when the intensity of that band is maximum (following the hypothesis from the previous Chapter that the band starts to decrease when all **2** molecules are bound and the average distance between them starts becoming larger), 2-3 equivalents of $\mathbf{1}_6$ are required to bind each equivalent of **2**. Assuming that the total concentration of **1** is 50 times higher than the concentration of **2** (again, an arbitrary value, set in line with the experiments in Chapter 4 but which can be modified easily), maximum binding is reached when the concentration of $\mathbf{1}_6$ is 0.04 times the total concentration of **1**, and therefore the value of k_9 is approximately 20. (Figure 5.5a). Lastly, we decided to give k_{10} the same value as k_0, so small differences in inhibition would cause the oxidation rate to go over or under the reduction rate.

[3] We used data recorded at a higher temperature in order to have similar timescales for photooxidation and the dynamics of the $\mathbf{1}_n$ macrocycles. To be precise, the inhibition of the photooxidation by $\mathbf{1}_6$ should be determined again at this temperature too, since its value might differ from the theoretical one or the one determined at 25 °C.

[4] We decided not to include in this model the decrease in Φ_Δ from unbound **2** to **2** bound to $\mathbf{1}_3/\mathbf{1}_4$. This model assumes that there are always enough $\mathbf{1}_n$ macrocycles to bind all **2**, which should be true except for conditions where almost all disulfides are reduced.

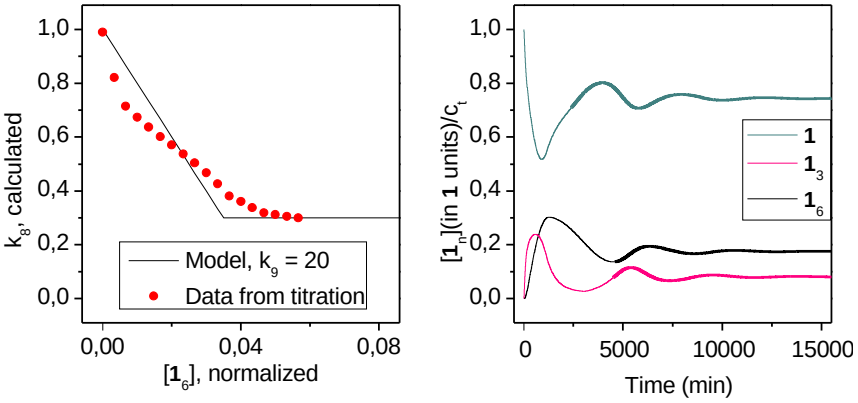

(a) Relative rate of photooxidation (k_8), in the model and calculated from experimental data (See main text for calculations)

(b) Initial model showing damped oscillations

Figure 5.5: (a) k_8 at different concentrations of $\mathbf{1}_6$ for k_9 = 20 (black) and data calculated from a titration of **2** with $\mathbf{1}_6$ (red, [**2**] = 4 µM, see main text and *Methods* for the calculation and the assumptions made) (b) Simulated concentrations of **1**, $\mathbf{1}_3$ and $\mathbf{1}_6$ using the parameters from Table 5.4c

We simulated this set of reactions using Berkeley Madonna (a software for numerically solving differential equations), and were pleased to observe damped oscillations of all the components of the system (except DTT). These oscillations had periods of around ~60 h and amplitudes that decreased progressively until they stopped being detectable after three oscillations (Figure 5.5b). Damped oscillations such as these are no proof that the system can achieve sustained oscillations [20], but in some cases oscillators have been reported to transition from damped to sustained after balancing the different parameters of the system [19].

Therefore, we decided to explore the parameter space of the model taking these initial values as a starting point. An attractive feature of the oscillator that is described here is that several of its constants can be modified independently. This allows for a thorough exploration of the parameter space, without the limitations that are intrinsic to other oscillators. Herein, we describe the constants that should be experimentally accessible, and show the effect that changing them had in the model.

- The simplest way of tuning this system is to change k_{10}: the rate at which DTT is flown in is simply a parameter of the syringe pump setup. Our model shows that when the value of k_{10} differs too much from k_0, oscillations decrease in amplitude and/or are completely lost. (Figure 5.6a) As expected, oscillations can only take place when the rate of oxidation is sim-

ilar to the combined rates of reduction, as the small differences caused by k_8 are enough to change from a reductive to an oxidative regime.

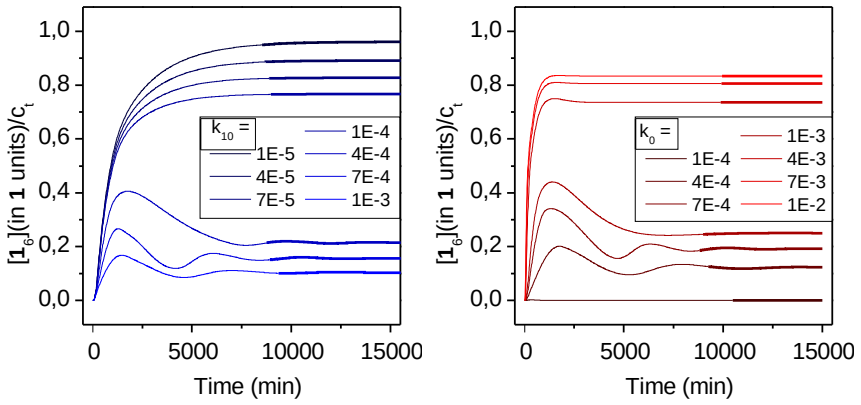

(a) Simulations varying k_{10} (Inflow of DTT). $k_0 = 6\times10^{-4}$

(b) Simulations varying k_0 (photooxidation rate). $k_{10} = 6\times10^{-4}$

Figure 5.6: Initial exploration of the parameter space of the oscillator using the numerical model. (a): k_0 is kept constant, and k_{10} varies. (b): k_{10} is kept constant, and k_0 varies. The values for the rest of parameters are kept as in Table 5.4c. The plots represent the total concentration of $\mathbf{1}_6$, in **1** units.

- k_0 can be modified by changing the intensity of the LEDs used to irradiate the system.[5] Naturally, the same effect is observed when changing this parameter as when changing k_{10}: In order for oscillations to take place, both values need to be of the same order of magnitude (Figure 5.6b).

- When changing k_0 and k_{10} together, we observe that, in general, an increase in both constants leads to oscillations with higher amplitude and lower period. However, this is only true for a certain range, and increasing both values beyond a certain threshold leads to a steady state after an initial wave of high hexamer concentration (Figure 5.7)

- k_9 is only defined as a parameter that controls the shape of the function correlating oxidation rate and the concentration of $\mathbf{1}_6$ in fibres. Therefore, it does not directly represent a real value. However, as it was mentioned above, it describes how sharp is the transition between "uninhibited" and "completely inhibited" oxidation. Experimentally, this transition would be

[5] Unlike k_{10}, we expect the value of k_0 to have some limitations: if it is too low, oxidation mediated by $^3O_2$ will play a role, and if it is too high, side-products such as sulphoxides or sulphones will form.

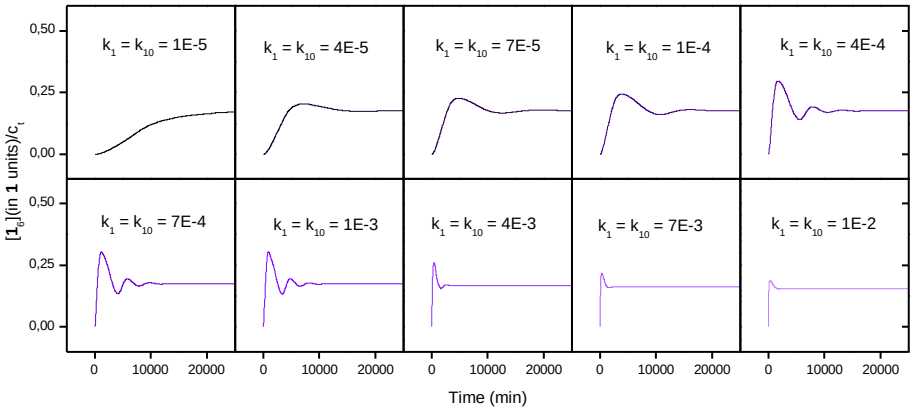

Figure 5.7: Simulations varying k_0 (photooxidation rate) and k_{10} (DTT inflow) together. Only the concentration of $\mathbf{1}_6$ is shown.

sharper the higher the ratio between **1** and **2**. Therefore, the experimental equivalent of "higher values of k_9" could be achieved by decreasing the concentration of **2**.[6] In our model, we observe that increasing the value of k_9 leads to sharper oscillations for longer periods of time, and a lower concentration of $\mathbf{1}_6$ in the steady state (Figure 5.8).

- Next, we studied the effect of changing the value of k_{11}, the relative reduction rate of $\mathbf{1}_6$ fibres. This parameter should be particularly important to oscillations, as it is the main mechanism through which the negative and positive feedback loops are decoupled from each other - the slower $\mathbf{1}_6$ is reduced (compared to $\mathbf{1}_3/\mathbf{1}_4$), the longer it will take between its emergence and its reduction. As it was shown above (Figures S5.5 and S5.6), the ratio between k_{11} and k_2 can be modified experimentally by using different reducing agents, and to a lower extent by using different stirring rates (which would result in fibres of different lengths). Our results show that, indeed, as the value of k_{11} decreases, the oscillations grow in amplitude and have a longer period (Figure S5.7)

- Lastly, we studied the effect of changing the minimum value of k_8 - the maximum inhibition that $\mathbf{1}_6$ can cause in photooxidation. Experimentally, we found a value for it between 0.4 and 0.6 (Figure 5.3d), higher than the one calculated from differences in Φ_Δ, 0.3. Our model shows that this

[6] This would decrease the value of k_0, but it could be compensated by increasing the intensity of the irradiation source (at least for a certain range of values).

value is critical: simulations where it is over 0.40 show practically no oscillations (Figures 5.9 and S5.8). The difference in Φ_Δ is an intrinsic property of the system and it cannot be modified experimentally. However, in order to make the maximum inhibition be as close to this value as possible, we should ensure that most oxidation is mediated by $^1O_2$. High concentrations of **2** and intense light sources should contribute to this, but could also cause overoxidation.

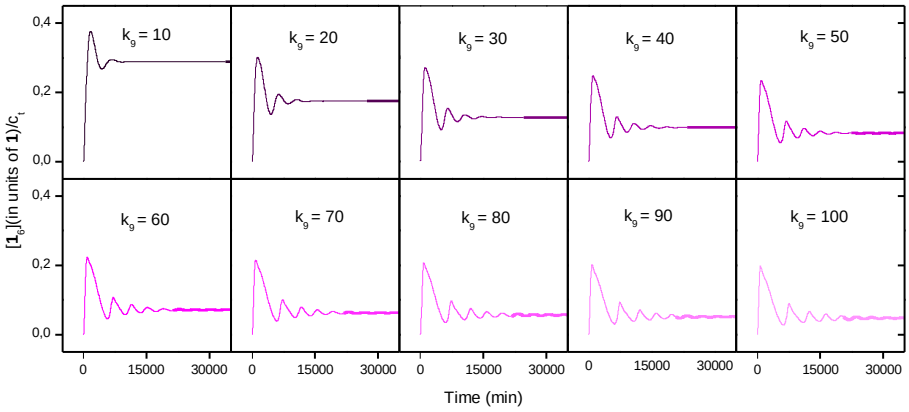

Figure 5.8: Simulations varying k_9, the parameter controlling the inhibition of photooxidation by $\mathbf{1}_6^{fib}$. Only the concentration of $\mathbf{1}_6$ is shown.

To summarize, the model confirms that a critical parameter for oxidation is the difference in rates between uninhibited and completely inhibited oxidation: the minimum value of k_8. According to the model, the experimentally determined value for this parameter is on the limit between showing and not showing oscillations, therefore it should be accurately determined and reduced, if possible. Besides this, there seems to be a trend where oscillations are more pronounced as the rates of photooxidation and reduction increase, as the inhibition takes place over a smaller range of $\mathbf{1}_6$ concentrations, and as the difference in reduction rates between $\mathbf{1}_6^{fib}$ and $\mathbf{1}_3/\mathbf{1}_4$ is higher.

Significantly, all oscillations observed here are damped: the concentration of $\mathbf{1}_6$ accumulates after each cycle until it reaches a steady state. This made us wonder if this steady state was unique or the system showed bistability. Bistability, as discussed previously, is intimately related to oscillations, so we performed preliminary simulations to study whether the $\mathbf{1}_n$ system would show it. Simulations starting from $\mathbf{1}_3/\mathbf{1}_4$ or $\mathbf{1}_6^{fib}$ led to the same steady state, with and without inhibition (Figures S5.9 and S5.10a), and under high inflow of DTT (Figure S5.10b).

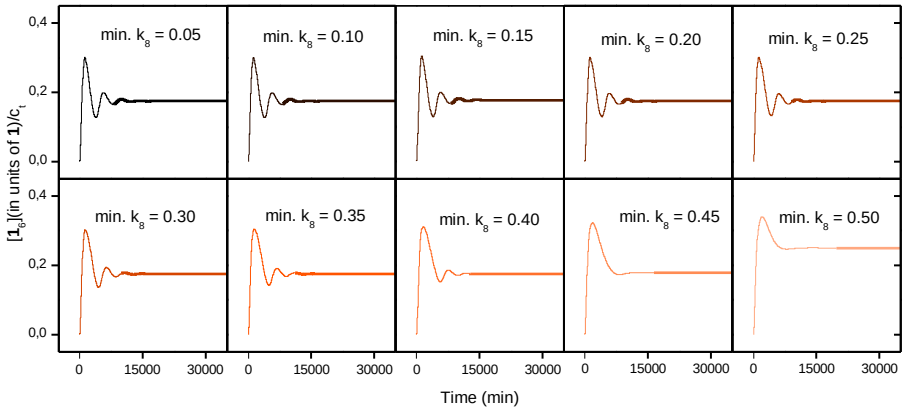

Figure 5.9: Simulations varying the minimum value of k_8 (limit to the inhibition of photooxidation by $\mathbf{1}_6$). Only the concentration of $\mathbf{1}_6$ is shown.

This indicates that the system is not bistable in the conditions screened - if it was, a different steady state would be reached when starting from the replicator or from non-replicating species. The most common way of achieving bistability in the literature - to have a continuous inflow and outflow of material, did not seem to improve the dampening or achieve bistability, either (Figure S5.11).

5.4 Conclusions

In this chapter, we designed an oscillator based on the $\mathbf{1}_n$ + **2** system. This design hinged on two key properties of the system: the autocatalysis of $\mathbf{1}_6$ and its inhibition of the photooxidation reaction catalysed by **2**. The first one has been previously established [24], and the second one was predicted by the results obtained in Chapter 4. Here, we confirmed this inhibition experimentally, although to a lower extent than what could be predicted from the ratios between the $^1O_2$ quantum yields (Φ_Δ) of **2** - the experimental decrease value was a factor of 2.1 $\pm$ 0.5, compared to the theoretical one of 3. The difference is probably due to experimental factors, such as oxidation mediated by other reactive oxygen species.

The system was then simulated using a kinetic model. We did observe oscillations in these simulations, but it should be remarked that those oscillations were always damped: the initial state was never completely restored after each cycle and all the conditions led eventually to a stationary state. Furthermore, this stationary state was always the same for each combination of constants, independently of the starting conditions - we have not been able to find conditions where

the system is bistable, either. Most of the oscillators that have been described experimentally achieve bistability by using a CSTR - a reactor with a continuous inflow and outflow of material. In our original design, the inflow of reducing agent should play that role (as shown in *Preliminary results*), but it might be interesting to explore CSTR-like setups in future research. At the end of this chapter we tentatively performed simulations in this direction, by adding an inflow of **1** and an outflow to the previous model. Only few simulations were done in this way, but they did not show bistability or sustained oscillations either. Lacking more parameter exploration or a deeper mathematical analysis (such as sensitivity analysis [25]), it is hard to conclude whether sustained oscillations would be possible with other parameter combination, or if the damping is inherent to the system, as it has been described for others [20, 26].

About the damped oscillations observed in the model, the results obtained here are at the same time encouraging and cautioning about their experimental realization. On one hand, these oscillations can be observed with a model that, despite not being carefully fitted, represents the behaviour of the $\mathbf{1}_n$ quite realistically. On the other hand, the experimental value of the inhibition of photooxidation by $\mathbf{1}_6$ is very close to the limit between damped oscillations and no oscillations (Figures 5.3d and 5.9), with the experimental error being under and over that threshold. This inhibition should be accurately determined and optimized to be as pronounced as possible: changing the temperature, concentration of **2**, and light intensity seem like promising candidates to affect it.

Further effort will be required in order to convert this design into a full-fledged oscillator (damped or sustained). However, this work showcases a completely new design for an oscillator in a competitive field where systems based on new principles are still scarce, despite abiological oscillating reactions existing for around a century.

5.5 Further experiments

We normally study the libraries of $\mathbf{1}_n$ macrocycles through UPLC analysis, as this method allows us to identify and quantify each of the macrocycles independently. However, experimental setups such as the one that would be necessary for oscillations (involving a syringe pump and a LED) cannot be easily coupled to commercially available UPLC systems. Due to the long experiment times (in the order of days) that the model predicts, periodically preparing aliquotes of the libraries becomes inconvenient, and it would be preferable to have an analytical tool able to monitor the composition of the library in a continuous way. In this chapter, we have already used UV/Vis spectroscopy to study the concentration of **1**, since it shows a different absorption band than its disulfide counterparts (Figure S5.4). In normal conditions, the absorbance spectrum of $\mathbf{1}_6$ is very similar to the spectrum of $\mathbf{1}_3/\mathbf{1}_4$ and they cannot be distinguished by UV/Vis. However,

in this particular case **2** is present in the solution too, so we predicted that we could use its J-band to quantify the concentration of $\mathbf{1}_6$.

We demonstrated this by setting up an irradiated seeding experiment containing **1**, $\mathbf{1}_6$ and **2** and following it by UPLC and UV/Vis (Figure 5.10a). The concentration of $\mathbf{1}_6$ was determined from the absorbance at 587 nm, and the concentration of **1** was determined from the ratio between the absorbances at 350 and 320 nm (at high concentrations of **2** precipitation starts to become a problem, so this parameter is more reliable than using only the absorbance at 350 nm). We converted these absorbances into concentrations by linear transformation in order to fit the ones determined by UPLC, and calculated the percentage of $\mathbf{1}_3/\mathbf{1}_4$ by difference with the others. As shown in Figure 5.10a, this analysis yielded a very good fit of the data, at least for **1** and $\mathbf{1}_6$ (R^2 = 0.98 and >0.99, respectively). A limitation of this analysis protocol is shown in the emergence experiment from Figure 5.10b: it does not work correctly once that the concentration of $\mathbf{1}_6$ is high enough to bind all **2** (dashed line). However, for relatively low concentrations of $\mathbf{1}_6$, it should provide an accurate and easy readout of the concentrations of the main species of the system, facilitating experiments that cannot be easily performed by UPLC analysis.

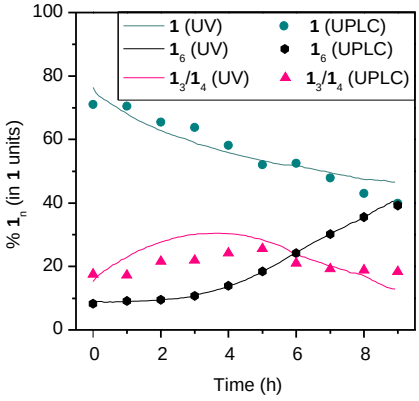

(a) Analysis of an irradiated library containing **1**, $\mathbf{1}_6$ and **2**, monitored both by UPLC and UV/Vis.

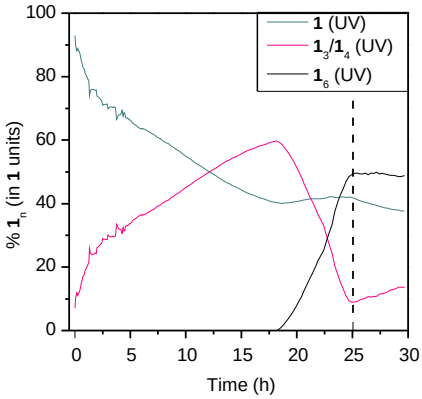

(b) Emergence of $\mathbf{1}_6$ in an irradiated library containing **1** and **2**, monitored by UV/Vis.

Figure 5.10: UV/Vis as an analytical tool for $\mathbf{1}_n$ libraries. (a) Seeding experiment monitored both by UPLC and UV-Vis. The library initially contained **1** (500 µM), **2** (25 µM), and $\mathbf{1}_6$ (50 µM). The absorbances at 587 nm and the ratio between 350 and 320 nm were transformed into the concentrations of $\mathbf{1}_6$ and **1**, respectively, using linear transformation to fit the values obtained by UPLC (Figure S5.3). (b) Irradiated library initially containing **1** (500 µM) and **2** (25 µM), analysed by UV/Vis using the values determined in (a). Both libraries were kept at 40 °C and stirred at 1000 rpm, and irradiated using a 565 nm LED.

5.6 Materials and methods

All reagents, solvents, and buffer salts were purchased from commercial sources and used without further purification. Building block **1** (XGLKFK) was obtained from Cambridge Peptides Ltd (Birmingham, UK). Dye **2** was purchased from Sigma-Aldrich (Purity 95 %). The irradiation at 525 nm was performed with a LED purchased from Lucky Light (model LL-504PGC2E-G5-3DC), with a light intensity of 15000 mcd, a viewing angle of 18 °, emission wavelengths of 525 ± 20 nm, and a power dissipation of 100 mW, according to the supplier. The irradiation at 565 nm (used in *Further experiments*) was performed with a LED purchased from Kingbright (model L793GD), with a light intensity of 60 mcd, a viewing angle of 60 °, emission wavelengths of 565 ± 7 nm, and a power dissipation of 105 mW, according to the supplier. Both LEDs were purchased through a local distributor (OKAPHONE, The Netherlands), and connected to a 5 V power source using a homemade setup. The LEDs were either fitted directly on top of the UV cuvettes or held in position with a wire. UV-Vis spectra were recorded using a Jasco V-650 UV spectrophotometer. Solutions for UV, CD and fluorescence were prepared and measured in polystyrene cuvettes, from Brand GMBH (Werrheim, Germany), using the corresponding buffer as a blank.

Buffer preparation

All the samples in this chapter were prepared using borate buffer as a solvent, with a pH of 8.2 and a total concentration of 50 mM in boron atoms.This buffer was prepared from B_2O_3, purchased from Sigma-Aldrich (Purity $\geq$ 99.5%)

Preparation of 5

Compound **5** was prepared by reduction of its oxidized counterpart, $\mathbf{5}_2$, adding 1.0 equivalent of TCEP to a buffered solution of it. Solutions of **5** were used immediately to prevent them from oxidizing again.

UPLC analysis

UPLC analysis was performed on a Waters Acquity UPLC H-class, equipped with a PDA detector. All analyses were performed using a reversed-phase UPLC column (Aeris Peptide 1.7 µm XB-C18 x 2.10 mm, Phenomenex). The column temperature was kept at 35 °C, and the sample plate was kept at 25 °C, unless otherwise specified. UV absorbance was monitored at 254 nm. For each injection, 10 µL of sample was injected.

The following solvents and gradient were used for UPLC analysis. The flow rate was kept at 0.3 ml/h.

Time(min)	% MeCN / 0.1 % TFA	%H_2O/ 0.1 % TFA
0	10	90
1	10	90
1.3	25	75
3	28	72
11	40	60
11.5	95	5
12	95	5
12.5	10	90
17	10	90

Preparation of $\mathbf{1}_6$

Stock solutions of $\mathbf{1}_6$ were typically prepared by dissolving building block **1** in borate buffer to a final concentration of 4.0 mM, and stirring the library at 40 °C. The library was monitored by UPLC analysis until completion.

Preparation of 40 nm $\mathbf{1}_6$ fibres

Fibres of $\mathbf{1}_6$ were mechanically sheared using a modified protocol previously published by our group [27]. A 150 µL aliquot of a previously prepared solution of $\mathbf{1}_6$ (4.0 mM) was placed in a Couette cell (R_{cup} = 20.25 mm, R_{bob} = 20.00 mm, average radius (R) = 20.125 mm). The sample was mechanically sheared by rotation of the inner cylinder, with a frequency of 4000 rpm (corresponding to a shear rate of 33702 s^{-1}). The resulting fibres were used within 48 h of preparation.

Preparation of $\mathbf{1}_3/\mathbf{1}_4$

Stock solutions of oxidized **1** libraries, named "$\mathbf{1}_3/\mathbf{1}_4$" in the text by their two main components, were typically prepared by dissolving building block **1** in borate buffer, adding 1 equivalent of $NaBO_4$, and diluting the library to a final concentration of 4.0 mM in residues of **1**. The libraries were monitored by UPLC until completion, which was typically done in less than 1 hour.

Determination of reaction orders in the oxidation and reduction of 5-5_2

Stock solutions of **5**, $\mathbf{5}_2$, **2**, and TCEP were diluted with borate buffer to the final concentrations indicated in the text, and their reaction was monitored over time, following the absorbance at 412 nm by UV/Vis. In the reactions between TCEP and $\mathbf{5}_2$, the reaction was followed immediately after mixing, and in the ones containing **2**, after starting irradiation at 525 nm. The initial reaction rate was determined for each sample by linear regression and converted to µM/h using a calibration curve ($R^2 > 0.95$). At least two samples were measured in this way for each data point, and their average and standard deviation were measured. The errors reported in the text were calculated from that standard deviation and the fitting errors of the linear regression in each of the samples (in most cases, the fitting error was significantly smaller than the variation between samples and could be ignored). The logarithms of the initial rates were then plotted against the logarithm of the initial concentrations of each of the reagents to obtain their reaction orders by linear regression. For the oxidation of **5**, the initial concentrations were determined from the initial absorbances instead of using the calculated values, to prevent any effect due to the stock solutions being oxidized by air before the reaction started.

Dissipative formation of 5_2 in a photooxidation-reduction regime

Stock solutions of $\mathbf{5}_2$ and **2** were mixed in a UV cuvette to final concentrations of 100 and 10 µM, respectively, and the solution was irradiated with a 525 nm LED at 40 °C. TCEP was flown in from a 4 mM stock solution at a rate of 0.1 mL/h for two minutes in order to get closer to the steady state, and then at a rate of 0.005 mL/h. These values did not practically change the volume of the sample (1.000 to 1.008 mL), but enough TCEP was added to completely reduce all of $\mathbf{5}_2$ (108 µM). After 50 minutes, both irradiation and inflow were stopped and removed from the cuvette.

Determination of the relative photooxidation rates of 1 in presence of 2 and different 1_n macrocycles

Stock solutions of **1** and **2** were mixed to final concentrations of 200 and 4.0 µM, respectively, and irradiated at 25 °C using 525 nm light. The absorbance at 350 nm was monitored over time and its initial rate was fitted by linear regression. Three repeats of each sample were prepared, and the data shown in Figure 5.3d represents the average and the standard deviation of these three samples (the fitting error was not significant compared to the variation between samples).

Reduction of $\mathbf{1_n}$ macrocycles with TCEP and DTT

Stock solutions of $\mathbf{1}_n$, were diluted to the final concentrations indicated in the text using borate buffer, and the absorbance of **1** at 350 nm was monitored over time at 25 °C. DTT or TCEP were then added and mixed using a standard micropipette. The data points during the mixing were discarded (as the absorbance was incorrectly measured due to the presence of the pipette).

Kinetic model

The model is given as a set of differential equations of species and their reactions. It was numerically solved using the software Berkeley Madonna, version 9.1.18 (Berkeley Madonna, Inc.) - code in *Appendix*. The variables shown in the graphs as **1**, $\mathbf{1}_3$ and $\mathbf{1}_6$ are named "*A*", "*tri*", and "*hex*" in the code, respectively. The model itself is based on previous results by Omer Markovitch (unpublished). The values of parameters not related to photooxidation or reduction were set to match the behaviour of a library in borate buffer (pH = 8.2, 50 mM in borate ions) stirred at 1200 rpm at 40 °C, with an initial concentration of **1** of 200 µM. For the determination of the rest of the constants, see *Results and discussion*.

Analysis of $\mathbf{1_n}$ libraries by UV/Vis

Libraries containing **1**, **2**, and $\mathbf{1}_6$ were prepared in a plastic cuvette and stirred at 1000 rpm inside of the UV-spectrophotometer, while keeping temperature constant at 40 °C and recording full spectra of the solution periodically. For the calibration of the analytical protocol (Figure 5.10a), the library was also monitored by UPLC. Linear transformations, optimized by the least squares method in Excel with the Add-in *Solver*, were used to fit the UV data to the percentages determined by UPLC.

5.7 Supplementary material

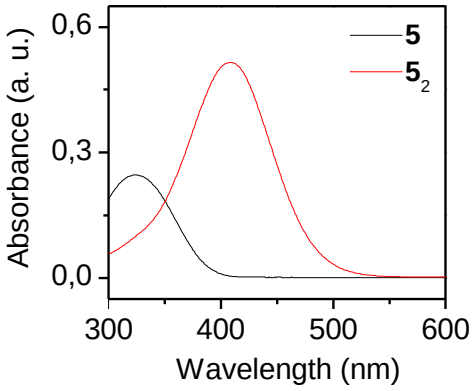

Figure S5.1: UV spectra of $\mathbf{5}_2$ before and after reduction with TCEP. The concentrations of $\mathbf{5}_2$ and TCEP were 20 µM, and the samples were prepared in borate buffer (pH = 8.2, 50 mM in boron atoms).

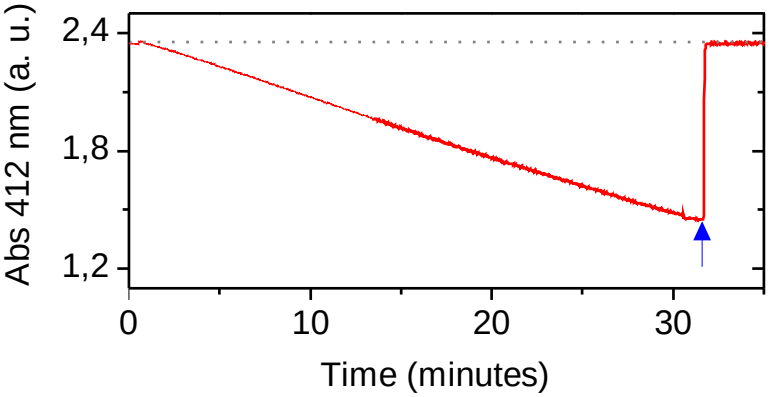

Figure S5.2: Reversibility of the oxidation of **5**. The sample was irradiated with a 525 nm LED for 31 minutes (blue arrow). After that, irradiation was turned off and the sample was completely reduced using TCEP. The concentration of **5** was 200 µM, the concentration of **2** was 10 µM and the concentration of TCEP was 110 µM. The dotted line indicates the original absorbance.

$$d[C]/dt = k \times [A]^a \times [B]^b$$
$$ln(d[C]/dt) = ln(k \times [B]^b) + a \times ln[A]$$
$$y = n + m \times x$$

(a) Initial rates method for the calculation of the reaction order of a reagent A in a A + B → C reaction where B is in excess.

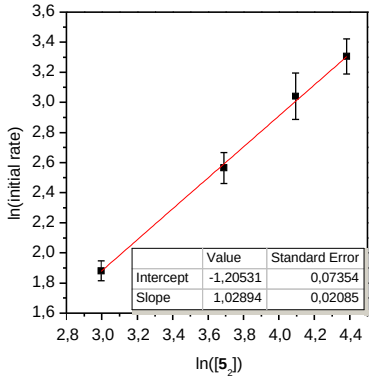

(b) Determination of the reaction order of $\mathbf{5}_2$ in the reduction reaction. [TCEP] = 200 µM, [$\mathbf{5}_2$] = 20-80 µM.

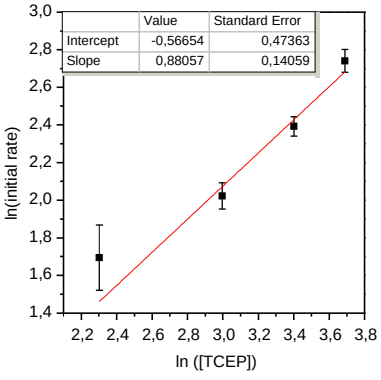

(c) Determination of the reaction order of TCEP in the reduction reaction. [$\mathbf{5}_2$] = 200 µM, [TCEP] = 10-40 µM.

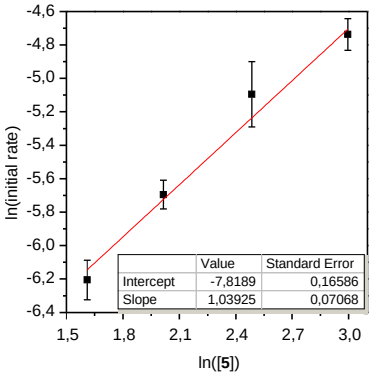

(d) Determination of the reaction order of **5** in the photooxidation reaction. [**2**] = 200 µM, [**5**] = 5-18 µM.

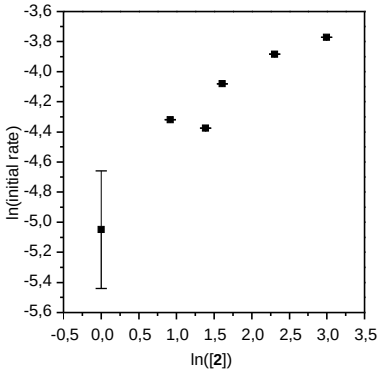

(e) Determination of the reaction order of **2** in the photooxidation reaction. [**5**] = 200 µM, [**2**] = 1-20 µM.

Figure S5.3: Determination of the reaction rates for the photooxidation and reduction of $\mathbf{5}_n$, using the initial rates method. Each point was calculated from 2 or 3 repeats. Error bars represent both the standard deviation between samples and the fitting error for the initial rates.

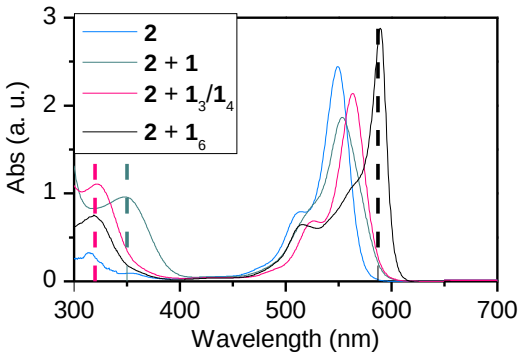

Figure S5.4: Spectra of combinations of **2** and different components of $\mathbf{1}_n$ libraries. The concentrations used to prepare the samples were 25 µM for **2** and 500 µM for $\mathbf{1}_n$. The dashed lines indicate the wavelengths used for quantifying the different species of the system during the chapter.

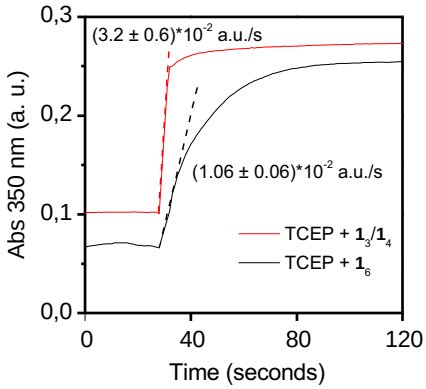

(a) Reduction of $\mathbf{1}_6$ or $\mathbf{1}_3/\mathbf{1}_4$ with TCEP.

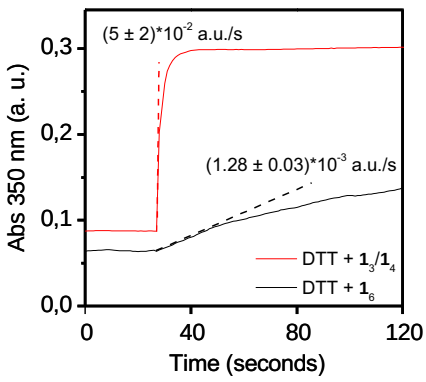

(b) Reduction of $\mathbf{1}_6$ or $\mathbf{1}_3/\mathbf{1}_4$ with DTT.

Figure S5.5: Reduction of $\mathbf{1}_n$ macrocycles using DTT and TCEP as reducing agents. The concentrations used were 200 µM of $\mathbf{1}_n$ macrocycles and 100 µM of reducing agent, borate buffer (pH = 8.2, 50 mM) was used as a solvent, and the temperature of the experiment was 25 °C.

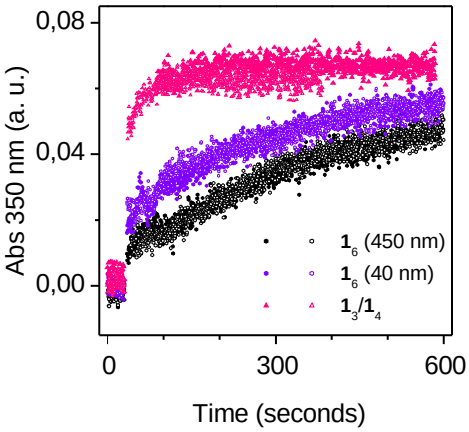

Figure S5.6: Reduction of $\mathbf{1}_3/\mathbf{1}_4$ and $\mathbf{1}_6$ fibres with different average lengths upon addition of DTT. The fibres labelled as 450 nm were prepared upon stirring at a speed of 1200 rpm using a magnetic stirrer, and the ones labelled as 40 nm were sheared at a speed of 4000 rpm using a couette cell [27]. All samples were prepared in duplicate, using borate buffer (pH = 8.2, 50 mM) as a solvent. Their temperature was set at 25 °C, and the final concentrations were 50 µM for both DTT and $\mathbf{1}_n$ macrocycles. The noise in the data is too high to calculate initial rates in this experiment, but a trend can be observed from the curves.

Reaction	Rate law
$3 \times \mathbf{1} \rightarrow \mathbf{1}_3$	$r_{ox} = k_1[\mathbf{1}]$
$\mathbf{1}_3 + 3 \times \mathbf{DTT} \rightarrow 3 \times \mathbf{1} + 3 \times \mathbf{DTT}_{ox}$	$r_{red3mer} = k_2[\mathbf{1}_3][\mathbf{DTT}]$
$2 \times \mathbf{1}_3 \rightarrow \mathbf{1}_6$	$r_{36} = k_3[\mathbf{1}_3]^2$
$2 \times \mathbf{1}_6 \rightarrow 4 \times \mathbf{1}_3$	$r_{63} = k_4[\mathbf{1}_6]^2$
$2 \times \mathbf{1}_6 \rightarrow 2 \times {\mathbf{1}_6}^{fib}$	$r_{emg} = k_5[\mathbf{1}_6]^2$
${\mathbf{1}_6}^{fib} + \mathbf{1}_6 \rightarrow 2 \times {\mathbf{1}_6}^{fib}$	$r_{elong} = k_6[{\mathbf{1}_6}^{fib}][\mathbf{1}_6]$
$\mathbf{1}_6 + 6 \times \mathbf{DTT} \rightarrow 6 \times \mathbf{1} + 6 \times \mathbf{DTT}_{ox}$	$r_{red6mer} = k_7[\mathbf{1}_6][\mathbf{DTT}]$
${\mathbf{1}_6}^{fib} + 6 \times \mathbf{DTT} \rightarrow 6 \times \mathbf{1} + 6 \times \mathbf{DTT}_{ox}$	$r_{redfib6mer} = k_{11}[{\mathbf{1}_6}^{fib}][\mathbf{DTT}]$
$\mathbf{DTT}_{stock} \rightarrow \mathbf{DTT}$	$r_{inflow} = k_{10}$

Table S5.1: Reactions simulated in the kinetic model

$$d[\mathbf{1}]/dt = -3r_{ox} + 3r_{red3mer} + 6r_{red6mer} + 6r_{redfib6mer}$$
$$d[\mathbf{1}_3]/dt = r_{ox} - r_{red3mer} - 2r_{36} + 4r_{63}$$
$$d[\mathbf{1}_6]/dt = r_{36} - 2r_{63} - 2r_{emg} - r_{elong} - r_{red6mer}$$
$$d[{\mathbf{1}_6}^{fib}]/dt = 2r_{emg} + r_{elong} - r_{red6fib}$$
$$d[\mathbf{DTT}]/dt = r_{inflow} - 3r_{red3mer} - 6r_{red6mer} - 6r_{redfib6mer}$$

Table S5.2: Differential equations of the model

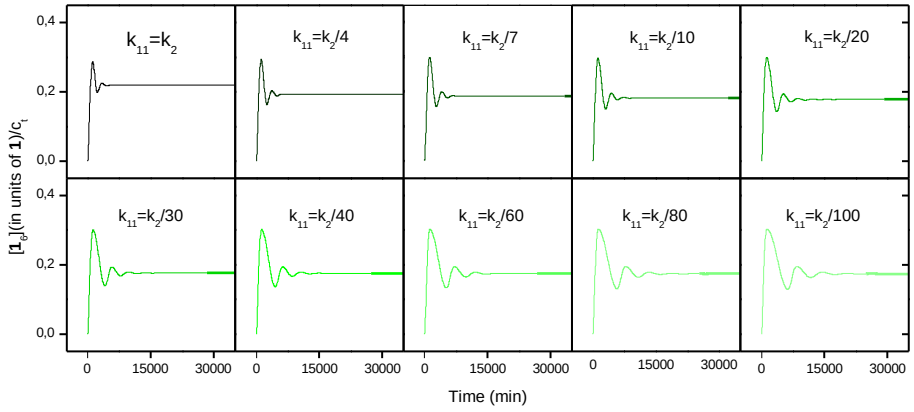

Figure S5.7: Simulations varying the value of k_{11} (reduction of $\mathbf{1}_6^{fib}$) as a function of k_2 (reduction of $\mathbf{1}_3$). Only the concentration of $\mathbf{1}_6$ is shown.

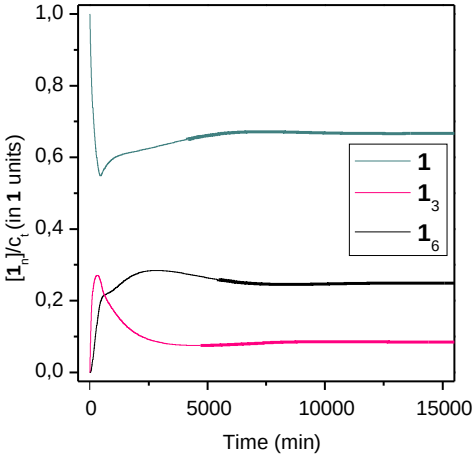

Figure S5.8: Simulation of the system setting 0.5 as the minimum value for k_8, and all other parameters to their optimal values as found in Figures 5.7 to S5.7. $k_0 = k_{10} = 1 \times 10^{-3}$, $k_{11}=k_2/100$, $k_9=100$.

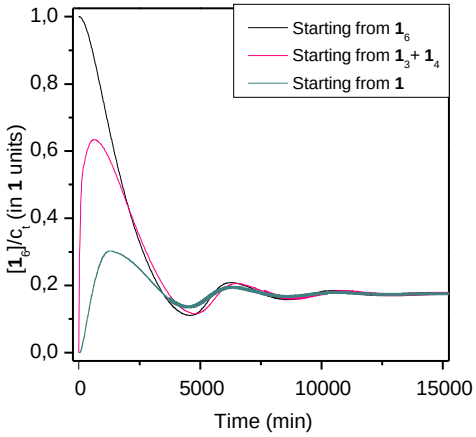

Figure S5.9: Simulations starting from 100 % of **1**, $\mathbf{1}_3/\mathbf{1}_4$, or $\mathbf{1}_6$

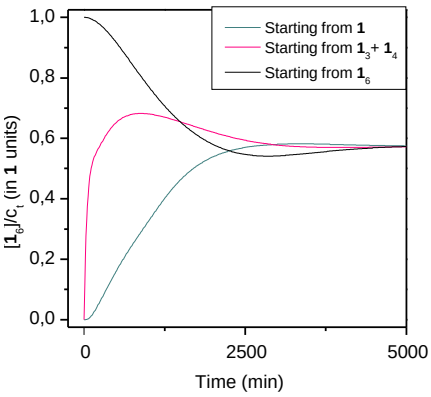

(a) Simulations starting from 100 % of **1**, $\mathbf{1}_3/\mathbf{1}_4$, or $\mathbf{1}_6$.

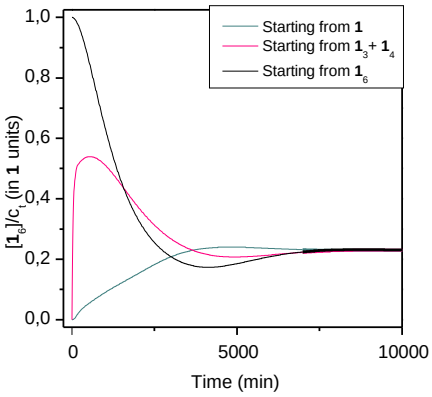

(b) Simulations without negative feedback and a high inflow of DTT starting from 100 % of **1**, $\mathbf{1}_3/\mathbf{1}_4$, or $\mathbf{1}_6$.

Figure S5.10: Checking for bistability in simulations of the model described in this chapter. The negative feedback was disabled by setting k_9 to 0. In panel (a), the value of k_{10} was not changed, and in panel (b) it was set to 1×10^{-3}. All other parameters were set to the values of Table 5.4c.

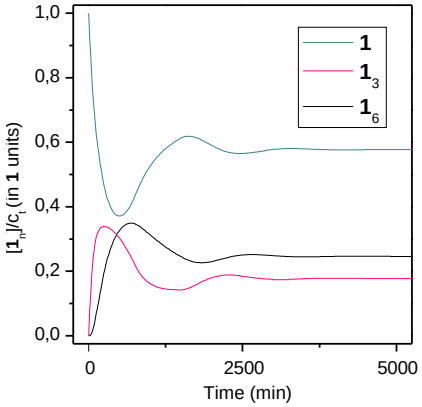

(a) Simulation adding an inflow and an outflow to the model described in Table S5.1.

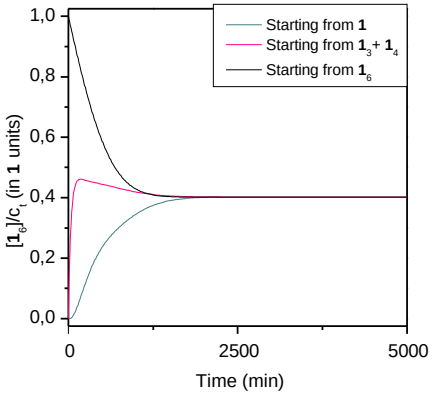

(b) Simulation with inflow and outflow and no negative feedback, starting from 100 % of **1**, $\mathbf{1}_3/\mathbf{1}_4$ or $\mathbf{1}_6$.

Figure S5.11: Simulations with constant inflow and outflow of material, as in a CSTR reactor. The flow rate used was 1×10^{-3} c_t/min, k_0 was increased to 1×10^{-3}, and the rest of the parameters were kept as in Figure 5.4c. In panel (a), k_9 was unchanged, but in panel (b) it was turned to 0 to disable the negative feedback loop. See *Appendix B* for the code of the model with inflow and outflow.

Concentration (In %, over 500 μM)	Linear transformation
$\%\mathbf{1}$	$101.75 \times Abs_{350}/Abs_{320} - 22.50$
$\%\mathbf{1}_6$	$24.69 \times Abs_{587} - 18.39$
$\%\mathbf{1}_3/\mathbf{1}_4$	$100 - \%\mathbf{1}_6 - \%\mathbf{1}$

Table S5.3: Linear transformations used to fit the absorbances observed in UV/Vis to the % of the different $\mathbf{1}_n$ species. These transformations were obtained from the data in Figure 5.10a, using the least squares method to minimize the differences between both methods.

5.7.1 Appendix A: Code of the kinetic model

```
METHOD RK4
STARTTIME = 0
STOPTIME = 50000
{A=monomer, B=3mer, C=6mer, D=6merfiber, E=DTT}
init A = 1
init B = 0
init C = 0
init D = 0
init E = 0
{Rates:} ox = k1*A
red3mer = k2*B*E
red6mer = k7*C*E
redfib6mer = k11*D*E
r36 = k3*B*B
r63 = k4*C*C
emg = k5*C*C
elong = k6*C*D
{Differential equations:}
d/dt(A) = - 3*ox + 3*red3mer + 6*red6mer + 6*redfib6mer
d/dt(B) = ox - red3mer - 2*r36 + 4*r63
d/dt(C) = r36 - 2*r63 - 2*emg - elong - red6mer
d/dt(D) = 2*emg + elong - redfib6mer
d/dt(E) = k10 - 3*red3mer - 6*red6mer - 6*redfib6mer
{Constants:}
k0 = 0.0006
k1 = k0* k8
k2 = 0.06
k3 = 0.02
k4 = 0.02
k5 = 0.01
k6 = 0.1
k7 = k2
k8 = MAX(0.3 , 1-k9*D)
k9 = 20
k10 = 0.0006
k11 = k2/40
{Variables for representation:} hex = 6*C + 6*D
tri = 3*B
total = A + 3*B + 6*C + 6*D
```

5.7.2 Appendix B: Code of the kinetic model including flow

```
METHOD RK4
STARTTIME = 0
STOPTIME = 50000
{A=monomer, B=3mer, C=6mer, D=6merfiber, E=DTT}
init A = 1
init B = 0
init C = 0
init D = 0
init E = 0
{Rates:} ox = k1*A
red3mer = k2*B*E
red6mer = k7*C*E
redfib6mer = k11*D*E
r36 = k3*B*B
r63 = k4*C*C
emg = k5*C*C
elong = k6*C*D
{Differential equations:}
d/dt(A) = kf - 3*ox + 3*red3mer + 6*red6mer + 6*redfib6mer
- kf*A
d/dt(B) = ox - red3mer - 2*r36 + 4*r63 - kf*B
d/dt(C) = r36 - 2*r63 - 2*emg -elong - red6mer - kf*C
d/dt(D) = 2*emg + elong - redfib6mer - kf*D
d/dt(E) = k10 - 3*red3mer - 6*red6mer - 6*redfib6mer- kf*E
{Constants:}kf = 0.001
k0 = 0.001
k1 = k0* k8
k2 = 0.06
k3 = 0.02
k4 = 0.02
k5 = 0.01
k6 = 0.1
k7 = k2
k8 = MAX(0.3 , 1-k9*D)
k9 = 20
k10 = 0.0006
k11 = k2/40
{Variables for representation:} hex = 6*C + 6*D
tri = 3*B
total = A + 3*B + 6*C + 6*D
```

5.8 Acknowledgements

Guillermo Monreal Santiago conceived the project, designed the system and determined the relevant kinetic constants. Leonard G. Cool performed the experiments related to **5**. Alexandre C. Walther developed the protocol for the UV analysis of $\mathbf{1}_n$. Guillermo Monreal Santiago and Omer Markovitch designed the model and performed numeric simulations. Sijbren Otto supervised the project, provided guidance, and helped shaping the direction of research. We thank Jim Ottelé for the experimental data of the **1** system at 40 °C, and Ivana Maric for the co-supervision of Leonard G. Cool. Xiaoming Miao is greatly acknowledged for proofreading the chapter.

5.9 References

[1] Whitesides, G. M.; Ismagilov, R. F. Complexity in chemistry. *Science* **1999**, *284*, 89–92.

[2] Semenov, S. N.; Kraft, L. J.; Ainla, A.; Zhao, M.; Baghbanzadeh, M.; Campbell, V. E.; Kang, K.; Fox, J. M.; Whitesides, G. M. Autocatalytic, bistable, oscillatory networks of biologically relevant organic reactions. *Nature* **2016**, *537*, 656–660.

[3] Wilhelm, T. The smallest chemical reaction system with bistability. *BMC Syst. Biol.* **2009**, *3*, 90.

[4] Aguda, B. D.; Clarke, B. L. Bistability in chemical reaction networks: theory and application to the peroxidase-oxidase reaction. *J. Chem. Phys.* **1987**, *87*, 3461–3470.

[5] Wagner, N.; Mukherjee, R.; Maity, I.; Peacock-Lopez, E.; Ashkenasy, G. Bistability and Bifurcation in Minimal Self-Replication and Nonenzymatic Catalytic Networks. *ChemPhysChem* **2017**, *18*, 1842–1850.

[6] Boissonade, J.; De Kepper, P. Transitions from bistability to limit cycle oscillations. Theoretical analysis and experimental evidence in an open chemical system. *J. Phys. Chem.* **1980**, *84*, 501–506.

[7] Grzybowski, B. A. *Chemistry in motion: reaction-diffusion systems for micro- and nanotechnology*; Wiley, 2009.

[8] Padirac, A.; Fujii, T.; Estévez-Torres, A.; Rondelez, Y. Spatial waves in synthetic biochemical networks. *J. Am. Chem. Soc.* **2013**, *135*, 14586–14592.

[9] Noyes, R. M.; Field, R. J. Oscillatory chemical reactions. *Annu. Rev. Phys. Chem.* **1974**, *25*, 95–119.

[10] Epstein, I. R.; Pojman, J. A. *An introduction to nonlinear chemical dynamics*; Oxford University Press: New York, 1998.

[11] Scott, S. K. *Oscillations, waves, and chaos in chemical kinetics*; Oxford University Press, 1994.

[12] Franck, U. F. Chemical oscillations. *Angew. Chemie Int. Ed. English* **1978**, *17*, 1–15.

[13] Domijan, M.; Kirkilionis, M. Bistability and oscillations in chemical reaction networks. *J. Math. Biol.* **2009**, *59*, 467–501.

[14] Craciun, G.; Tang, Y.; Feinberg, M. Understanding bistability in complex enzyme-driven reaction networks. *Proc. Natl. Acad. Sci. U. S. A.* **2006**, *103*, 8697–8702.

[15] Kurin-Csörgel, K.; Epstein, I. R.; Orbán, M. Systematic design of chemical oscillators using complexation and precipitation equilibria. *Nature* **2005**, *433*, 139–142.

[16] Montagne, K.; Plasson, R.; Sakai, Y.; Fujii, T.; Rondelez, Y. Programming an in vitro DNA oscillator using a molecular networking strategy. *Mol. Syst. Biol.* **2011**, *7*, 466.

[17] Novák, B.; Tyson, J. J. Design principles of biochemical oscillators. *Nat. Rev. Mol. Cell Biol.* **2008**, *9*, 981–991.

[18] Kovacs, K.; McIlwaine, R. E.; Scott, S. K.; Taylor, A. F. An organic-based pH oscillator. *J. Phys. Chem. A* **2007**, *111*, 549–551.

[19] Semenov, S. N.; Wong, A. S.; Van Der Made, R. M.; Postma, S. G.; Groen, J.; Van Roekel, H. W.; De Greef, T. F.; Huck, W. T. Rational design of functional and tunable oscillating enzymatic networks. *Nat. Chem.* **2015**, *7*, 160–165.

[20] Leira-Iglesias, J.; Tassoni, A.; Adachi, T.; Stich, M.; Hermans, T. M. Oscillations, travelling fronts and patterns in a supramolecular system. *Nat. Nanotechnol.* **2018**, *13*, 1021–1027.

[21] Ellman, G. L. Tissue sulfhydryl groups. *Arch. Biochem. Biophys.* **1959**, *82*, 70–77.

[22] Burns, J. A.; Butler, J. C.; Moran, J.; Whitesides, G. M. Selective reduction of disulfides by tris(2-carboxyethyl)phosphine. *J. Org. Chem.* **1991**, *56*, 2648–2650.

[23] Fava, A.; Iliceto, A.; Camera, E. Kinetics of the Thiol–Disulfide Exchange. *J. Am. Chem. Soc.* **1957**, *79*, 833–838.

[24] Colomb-Delsuc, M.; Mattia, E.; Sadownik, J. W.; Otto, S. Exponential self-replication enabled through a fibre elongation/breakage mechanism. *Nat. Commun.* **2015**, *6*.

[25] Wilkins, K.; Tidor, B.; White, J.; Barton, P. I. Sensitivity analysis for oscillating dynamical systems. *SIAM J. Sci. Comput.* **2009**, *31*, 2706–2732.

[26] Hammele, M.; Zimmermann, W. Modeling oscillatory microtubule polymerization. *Phys. Rev. E - Stat. Physics, Plasmas, Fluids, Relat. Interdiscip. Top.* **2003**, *67*, 19.

[27] Pal, A.; Malakoutikhah, M.; Leonetti, G.; Tezcan, M.; Colomb-Delsuc, M.; Nguyen, V. D.; Van Der Gucht, J.; Otto, S. Controlling the structure and length of self-synthesizing supramolecular polymers through nucleated growth and disassembly. *Angew. Chemie - Int. Ed.* **2015**, *54*, 7852–7856.